Inorg. Chem. **2009**, *48*, 2652−2663

An Iron Complex of Dipyridophenazine as a Potent Photocytotoxic Agent in Visible Light

Sounik Saha,[†] Ritankar Majumdar,[‡] Mithun Roy,[†] Rajan R. Dighe,[‡] and Akhil R. Chakravarty*[,†]

Department of Inorganic and Physical Chemistry and Department of Molecular Reproduction, Development and Genetics, Indian Institute of Science, Bangalore 560012, India

Received November 25, 2008

Ternary iron(III) complexes [FeL(B)] (**1**−**3**) of a trianionic tetradentate phenolate-based ligand (L) and phenanthroline base (B), namely, 1,10-phenanthroline (phen, **1**), dipyridoquinoxaline (dpq, **2**), and dipyridophenazine (dppz, **3**), have been prepared and structurally characterized and their DNA binding, cleavage, and photocytotoxic properties studied. The complexes with a FeN_3O_3 core show the Fe(III)/Fe(II) redox couple near −0.6 V in DMF, a magnetic moment value of ∼5.9 μ_B, and a binding propensity to both calf thymus DNA and bovine serum albumin (BSA) protein. They exhibit red-light-induced DNA cleavage activity following a metal-assisted photoredox pathway forming $HO^{\bullet}$ radicals but do not show any photocleavage of BSA in UV-A light. Complex **3** displays photocytotoxicity in the human cervical cancer cell line (HeLa) and human keratinocyte cell line (HaCaT) with respective IC_{50} values of 3.59 μM and 6.07 μM in visible light and 251 nM and 751 nM in UV-A light of 365 nm. No significant cytotoxicity is observed in the dark. The photoexposed HeLa cells, treated prior with complex **3**, have shown marked changes in nuclear morphology as demonstrated by Hoechst 33258 nuclear stain. Generation of reactive oxygen species has been evidenced from the fluorescence enhancement of dichlorofluorescein upon treatment with **3** followed by photoexposure. Nuclear chromatin cleavage has been observed in acridine orange/ethidium bromide dual staining of treated HeLa cells and from alkaline single-cell gel electrophoresis. Caspase 3/7 activity in HeLa cells has been found to be upregulated by only 4 fold after photoirradiation, signifying the fact that cell death through a caspase 3/7 dependent pathway may not be solely operative.

Introduction

Photodynamic therapy (PDT) is an emerging noninvasive treatment modality for tumors.[1−10] It involves the simultaneous presence of light, oxygen, and photosensitizing drugs to achieve the photocytotoxic effect. The photosensitizer on irradiation within the PDT spectral window undergoes various reactions, among which electron transfer and energy transfer are the most prevalent ones. Radicals and singlet oxygen species produced by such processes are responsible for damaging cancer cells. Photofrin, the currently used PDT drug, is an oligomeric mixture of hematoporphyrin species, which on photoactivation at 633 nm generates a $^1(\pi-\pi^*)$ state with subsequent formation of a $^3(\pi-\pi^*)$ state that activates molecular oxygen to its cytotoxic singlet oxygen ($^1O_2$) species by energy transfer.[1] Porphyrin-based organic dyes suffer from skin sensitivity and hepatotoxicity, forming bilirubin on metabolic oxidation.[11,12] This has led to the development of the chemistry of nonporphyrinic organic dyes like phthalocyanins, texaphyrins, squaranines, boradiazain-

* To whom correspondence should be addressed. Tel.: +91-80-22932533. Fax: +91-80-23600683. E-mail: arc@ipc.iisc.ernet.in.
† Department of Inorganic and Physical Chemistry.
‡ Department of Molecular Reproduction, Development and Genetics.

(1) Bonnett, R. *Chemical Aspects of Photodynamic Therapy*; Gordon & Breach: London, U.K., 2000.
(2) Detty, M. R.; Gibson, S. L.; Wagner, S. J. *J. Med. Chem.* **2004**, *47*, 3897–3915.
(3) Henderson, B. W.; Busch, T. M.; Vaughan, L. A.; Frawley, N. P.; Babich, D.; Sosa, T. A.; Zollo, J. D.; Dee, A. S.; Cooper, M. T.; Bellnier, D. A.; Greco, W. R.; Oseroff, A. R. *Cancer Res.* **2000**, *60*, 525–529.
(4) Sternberg, E. D.; Dolphin, D.; Brückner, C. *Tetrahedron* **1998**, *54*, 4151–4202.
(5) DeRosa, M. C.; Crutchley, R. J. *Coord. Chem. Rev.* **2002**, *233*, 351–371.
(6) Stochel, G.; Wanad, A.; Kulis, E.; Stasicka, Z. *Coord. Chem. Rev.* **1998**, *171*, 203–220.
(7) Delaey, E.; Van Laar, F.; De Vos, D.; Kamuhabwa, A.; Jacobs, P.; De Witte, P. *J. Photochem. Photobiol., B* **2000**, *55*, 27–36.
(8) Ali, H.; Van Lier, J. E. *Chem. Rev.* **1999**, *99*, 2379–2450.
(9) Sessler, J. L.; Hemmi, G.; Mody, T. D.; Murai, T.; Burrell, A.; Young, S. W. *Acc. Chem. Res.* **1994**, *27*, 43–50.
(10) Bonnet, R.; Martinez, G. *Tetrahedron* **2001**, *57*, 9513–9547.

10.1021/ic8022612 CCC: $40.75
Published on Web 02/09/2009

dacenes, and so forth as potential near-infrared photosensitizers for PDT applications.[13−18] The organic dyes in general follow a mechanistic pathway that forms cytotoxic singlet oxygen molecules.[19] The ability to generate singlet oxygen on photoactivation within the PDT spectral window is thus of paramount importance for such organic dyes. To circumvent this limitation, transition metal complexes with their tunable coordination geometry and varied redox properties in the presence of low-energy d−d or charge transfer band(s) could offer a scope for developing metal-based PDT agents showing cellular damage following different mechanistic pathways.[20]

Cisplatin and its analogues have been successfully used as non-PDT metal-based anticancer drugs.[21−23] Current platinum-based chemotherapeutic drugs suffer from side effects along with drug-resistance-related problems. To overcome these problems, efforts are on to use platinum(IV) complexes that could release cisplatin or its analogues in cancer cells by intracellular reduction of the metal by photochemical or chemical means. Lippard and co-workers have reported platinum(IV) complexes designed for targeted drug delivery, releasing cisplatin upon intracellular reduction of the metal in the cancer cells.[24] Using a different approach in cancer chemotherapy, Sadler and workers have shown that a six-coordinate platinum(IV) complex as a photoactivatable metallodrug with two trans azide ligands is stable in the dark but generates a trans diguanidine platinum(II) adduct on photoactivation, killing human cancer cells.[25] In addition, there are reports on dirhodium(II,II) complexes showing photocytotoxic effects in visible light using different cancer cell lines.[26−28] $[RuCl_2(DMSO)_4]$ has been reported to be photoactivated by light in cells and hence behaves as a potent cytotoxin when irradiated with UV-A light.[29] UV-A light-induced cytotoxicity is reported for transplatin using human keratinocytes HaCaT and ovarian cancer A2780 cells.[30] Ruthenium nitrosyls have been used for the site-specific delivery of cytotoxic nitric oxide (NO) on exposure to visible light as a new modality in PDT.[31] Although the focus on metal-based drugs in PDT has primarily been on the heavy metals like platinum, ruthenium, and rhodium, the utility of bioessential 3d-transition metals like iron has remained virtually unexplored.[32,33]

Organic dyes used in PDT generally follow a singlet oxygen (type-II) mechanistic pathway.[19] In contrast, redox active 3d-metal complexes could cleave DNA in an oxidative manner through a photoredox pathway, generating hydroxyl radicals under aerobic conditions.[20,34−36] Designing metallodrugs in PDT has several basic requirements, namely, the biocompatibility of the metal ion, its redox activity and reversibility, photoactivity within the PDT spectral window, and DNA binding propensity. Our recent reports have shown that a dipyridoquinoxaline (dpq) complex of $3d^5$−iron(III) could photocleave DNA in visible light within the PDT spectral window, while the $3d^6$−iron(II) complex of dpq is photoinactive in visible light.[35,37] This observation has prompted us to explore the iron(III) complexes further by designing a series of ternary iron(III) complexes [FeL(B)] (**1**−**3**) as a new class of photoactive species having lipophilic tertiary butyl groups containing a tetradentate phenolate-based ligand (2-bis-[3,5-di(*tert*-butyl)-2-hydroxybenzyl]aminoacetic acid, H_3L) and DNA binding phenanthroline bases (B), namely, 1,10-penanthroline (phen, **1**), dipyrido[3,2-d:2′,3′-f]quinoxaline (dpq, **2**), and dipyrido[3,2-a:2′,3′-c]phenazine (dppz, **3**), to study their photocytotoxic properties in visible light using different cancer cell lines (Scheme 1). To facilitate the metal-assisted photoinduced DNA cleavage activity in visible light, we have used the DNA binding phenanthroline bases having quinoxaline and phenazine moieties that are present in antitumor antibiotics like echi-

(11) Ochsner, M. *J. Photochem. Photobiol., B* **1996**, *32*, 3–9.
(12) Moriwaki, S. I.; Misawa, J.; Yoshinari, Y.; Yamada, I.; Takigawa, M.; Tokura, Y. *Photodermatol. Photoimmunol. Photomed.* **2001**, *17*, 241–243.
(13) Wei, W.-H.; Wang, Z.; Mizuno, T.; Cortez, C.; Fu, L.; Sirisawad, M.; Naumovski, L.; Magda, D.; Sessler, J. L. *Dalton Trans.* **2006**, 1934–1942.
(14) Rodriguez, M. E.; Moran, F.; Bonansea, A.; Monetti, M.; Fernandez, D. A.; Strassert, C. A.; Rivarola, V.; Awruch, J.; Dicelio, L. E. *Photochem. Photobiol. Sci.* **2003**, *2*, 988–994.
(15) Ramaiah, D.; Eckert, I.; Arun, K. T.; Weidenfeller, L.; Epe, B. *Photochem. Photobiol.* **2004**, *79*, 99–104.
(16) Kar, M.; Basak, A. *Chem. Rev.* **2007**, *107*, 2861–2890.
(17) Verma, S.; Watt, G. M.; Mai, Z.; Hasan, T. *Photochem. Photobiol.* **2007**, *83*, 996–1005.
(18) Atilgan, S.; Ekmeckci, Z.; Dogan, A. L.; Guc, D.; Akkaya, E. U. *Chem. Commun.* **2006**, 4398–4400.
(19) Szaciłowski, K.; Macyk, W.; Drzewiecka-Matuszek, A.; Brindell, M.; Stochel, G. *Chem. Rev.* **2005**, *105*, 2647–2694.
(20) (a) Burrows, C. J.; Muller, J. G. *Chem. Rev.* **1998**, *98*, 1109–1151. (b) Meunier, B.; Pratviel, G.; Bernadou, J. *Bull. Soc. Chim. Fr.* **1994**, *131*, 933–943. (c) Armitage, B. *Chem. Rev.* **1998**, *98*, 1171–1200.
(21) Rosenberg, B.; VamCamp, L.; Trosko, J. E.; Mansour, V. H. *Nature* **1969**, *222*, 385–386.
(22) (a) Zhang, C. X.; Lippard, S. J. *Curr. Opin. Chem. Biol.* **2003**, *7*, 481–489. (b) Lippard, S. J. *Biochemistry* **2003**, *42*, 2664–2671. (c) Jamieson, E. R.; Lippard, S. J. *Chem. Rev.* **1999**, *99*, 2467–2498.
(23) (a) Galanski, M.; Jakupec, M. A.; Keppler, B. K. *Curr. Med. Chem.* **2005**, *12*, 2075–2079. (b) Kang, H. C.; Kim, I.-J.; Park, H.-W.; Jang, S.-G.; Ahn, S.-A.; Yoon, S. N.; Chang, H. J.; Yoo, B. C.; Park, J.-G. *Cancer Lett.* **2007**, *247*, 40–47.
(24) (a) Dhar, S.; Liu, Z.; Thomale, J.; Dai, H.; Lippard, S. J. *J. Am. Chem. Soc.* **2008**, *130*, 11467–11476. (b) Dhar, S.; Gu, F. X.; Langer, R.; Farokhzad, O. C.; Lippard, S. J. *Proc. Natl. Acad. Sci. U. S. A.* **2008**, *105*, 17356–17361.
(25) Mackay, F. S.; Woods, J. A.; Heringová, P.; Kašpárková, J.; Pizarro, A. M.; Moggach, S. A.; Parsons, S.; Brabec, V.; Sadler, P. J. *Proc. Natl. Acad. Sci. U. S. A.* **2007**, *104*, 20743–20748.
(26) Chifotides, H. T.; Dunbar, K. R. *Acc. Chem. Res.* **2005**, *38*, 146–156.
(27) Angeles-Boza, A. M.; Chifotides, H. T.; Aguirre, J. D.; Chouai, A.; Fu, P. K.-L.; Dunbar, K. R.; Turro, C. *J. Med. Chem.* **2006**, *49*, 6841–6847.
(28) (a) Angeles-Boza, A. M.; Bradley, P. M.; Fu, P. K.-L.; Wicke, S. E.; Bacsa, J.; Dunbar, K. R.; Turro, C. *Inorg. Chem.* **2004**, *43*, 8510–8519. (b) Bradley, P. M.; Angeles-Boza, A. M.; Dunbar, K. R.; Turro, C. *Inorg. Chem.* **2004**, *53*, 2450–2452.
(29) Brindell, M.; Kuliś, E.; Elmroth, S. K.; Urbańska, K.; Stochel, G. *J. Med. Chem.* **2005**, *48*, 7298–7304.
(30) Heringová, P.; Woods, J.; Mackay, F. S.; Kašpárková, J.; Sadler, P. J.; Brabec, V. *J. Med. Chem.* **2006**, *49*, 7792–7798.
(31) Rose, M. J.; Fry, N. L.; Marlow, R.; Hinck, L.; Mascharak, P. K. *J. Am. Chem. Soc.* **2008**, *130*, 8834–8846.
(32) Boerner, L. K. J.; Zaleski, J. M. *Curr. Opin. Chem. Biol.* **2005**, *9*, 135–144.
(33) Kraft, B. J.; Zaleski, J. M. *New J. Chem.* **2001**, *25*, 1281–1289.
(34) Dhar, S.; Senapati, D.; Reddy, P. A. N.; Das, P. K.; Chakravarty, A. R. *Chem. Commun.* **2003**, 2452–2453.
(35) Roy, M.; Pathak, B.; Patra, A. K.; Jemmis, E. D.; Nethaji, M.; Chakravarty, A. R. *Inorg. Chem.* **2007**, *46*, 11122–11132.
(36) Maity, B.; Roy, M.; Chakravarty, A. R. *J. Organomet. Chem.* **2008**, *693*, 1395–1399.
(37) Roy, M.; Saha, S.; Patra, A. K.; Nethaji, M.; Chakravarty, A. R. *Inorg. Chem.* **2007**, *46*, 4368–4370.

Scheme 1. Schematic Drawings of the Complexes and the Ligands Used

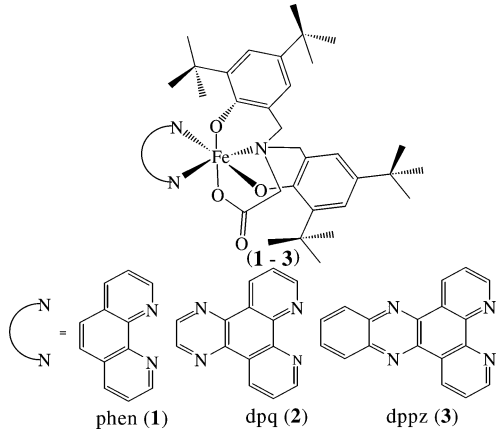

nomycin or triostin.[38,39] Such moieties are known to generate photoexcited $^3(n-\pi^*)$ or $^3(\pi-\pi^*)$ state cleaving DNA on photoirradiation with UV light.[38] Herein, we report the DNA binding and photoinduced DNA cleavage activity of the ternary iron(III) complexes **1**−**3**. Among these three complexes, the dppz complex **3** has been found to show low dark toxicity in the presence of cellular reducing agent glutathione and remarkably high photocytotoxicity in visible light (400−700 nm). Rapid induction of cell death following an apoptotic pathway within 2 h of photoirradiation has been noticed, which provides a marked advantage over conventional chemotherapy. A preliminary communication on the structure and plasmid DNA cleavage activity of the dpq complex **2** has been made.[37]

Experimental Section

Materials and Measurements. The reagents and chemicals were procured from commercial sources (Sigma-Aldrich, U. S. A.; SD Fine Chemicals, India) and used as received without further purification. The solvents used were purified using standard procedures.[40] Supercoiled (SC) pUC19 DNA (cesium chloride purified) was purchased from Bangalore Genei (India). Calf thymus (CT) DNA, bovine serum albumin (BSA), agarose (molecular biology grade), distamycin-A, catalase, superoxide dismutase (SOD), 2,2,6,6-tetramethyl-4-piperidone (TEMP), 2′,7′-dichlorofluorescein diacetate (DCFH-DA), Hoechst 33258, and ethidium bromide (EB) were from Sigma (U. S. A.). Tris(hydroxymethyl)aminomethane−HCl (Tris-HCl) buffer was prepared using deionized and sonicated triple-distilled water. The *N*,*N*-donor heterocyclic bases, dpq and dppz, were prepared according to literature procedures using 1,10-phenanthroline-5,6-dione as a precursor reacted with ethylenediamine for dpq and 1,2-phenylenediamine for dppz.[41,42] The ligand H_3L was prepared following a literature procedure.[43]

The elemental analysis was done using a Thermo Finnigan FLASH EA 1112 CHNS analyzer. The infrared and electronic spectra were recorded on PerkinElmer Lambda 35 and PerkinElmer spectrum one 55 spectrophotometers, respectively. Magnetic susceptibility data for polycrystalline samples of the complexes were obtained using a model 300 Lewis-coil-force magnetometer of George Associates, Inc. (Berkeley, U. S. A.) make. $Hg[Co(NCS)_4]$ was used as a standard. Experimental susceptibility data were corrected for diamagnetic contributions.[44] Molar conductivity measurements were done using a Control Dynamics (India) conductivity meter. Cyclic voltammetric measurements were made at 25 °C using an EG&G PAR 253 VersaStat potentiostat/galvanostat with a three-electrode configuration consisting of a glassy carbon working, a platinum wire auxiliary, and a saturated calomel reference (SCE) electrode. Ferrocene ($E_{1/2} = 0.42$ V) was used as a standard in MeCN−0.1 M $[Bu_4^nN](ClO_4)$ (TBAP). Electrospray ionization mass and ^{1}H NMR spectral measurements were made using Bruker Daltonics make (Esquire 300 Plus ESI Model) and Bruker 400 MHz NMR spectrometers, respectively. Fluorescence microscopic investigations were carried out on a Leica DM IL microscope with an integrated Leica DFC 320 R2 camera and IL50 image software.

Synthesis of [FeL(B)] (B = phen, 1; dpq, 2; dppz, 3). The complexes were prepared using a general procedure in which the ligand H_3L (0.255 g, 0.5 mmol) taken in a mixture of MeOH, EtOH, and MeCN (3:3:2 v/v, 20 mL) was reacted with Et_3N (0.2 mL, 1.5 mmol) followed by the addition of $Fe(NO_3)_3\cdot 9H_2O$ (0.202 g, 0.5 mmol). The solution was stirred for 15 min, followed by the addition of phenanthroline base B (0.099 g, phen; 0.116 g, dpq; 0.141 g, dppz; 0.5 mmol). The solution was filtered after 10 min. The filtrate on slow evaporation gave dark purple block-shaped crystals in analytically pure form.

[FeL(phen)] (1). Yield: 68% (0.253 g). Anal. calcd for $C_{44}H_{54}FeN_3O_4$: C, 70.96; H, 7.31; N, 5.64. Found: C, 70.71; H, 7.48; N, 5.72. Molar conductance in DMF (Λ_M): 12 S m^2 M^{-1}. FT-IR (KBr phase): 2949vs, 1660vs (ν_{coo}), 1515s, 1468m, 1385s, 1306m, 1237s, 1168s, 1107w, 919m, 876w, 731s, 637w, 608w, 540m, 475m cm^{-1} (vs, very strong; s, strong; m, medium; w, weak). ESI-MS in MeCN: *m*/*z* 745.3 $(M + H)^+$. UV−vis in 6% DMF/Tris HCl buffer [λ_{max}, nm (ε, M^{-1} cm^{-1})]: 490 (5150), 372 (6610), 290 (38 300), 266 (46 150). μ_{eff} (298 K): 5.85 μ_B.

[FeL(dpq)] (2). Yield: 61% (0.243 g). Anal. calcd for $C_{46}H_{54}FeN_5O_4$: C, 69.34; H, 6.83; N, 8.79. Found: C, 69.15; H, 6.90; N, 9.01. Λ_M in DMF: 10 S m^2 M^{-1}. FT-IR (KBr phase): 2953vs, 1670vs (ν_{coo}), 1517s, 1468m, 1381s, 1307m, 1244s, 1168s, 1110w, 916m, 876w, 842m, 733s, 639w, 618w, 551m, 473m cm^{-1}. ESI-MS in MeCN: *m*/*z* 797.3 $(M + H)^+$. UV−vis in 6% DMF/Tris-HCl buffer [λ_{max}, nm (ε, M^{-1} cm^{-1})]: 470 (5150), 340 (16 600), 325 (18 700), 282 (39 800), 253 (71 700). μ_{eff} (298 K): 5.86 μ_B.

[FeL(dppz)] (3). Yield: 77% (0.325 g). Anal. calcd for $C_{50}H_{56}FeN_5O_4$: C, 70.91; H, 6.67; N, 8.27. Found: C, 70.64; H, 6.58; N, 8.52. Λ_M in DMF: 16 S m^2 M^{-1}. FT-IR (KBr phase): 2952vs, 1667vs (ν_{coo}), 1520s, 1468m, 1383s, 1304m, 1243s, 1169s, 1112w, 913m, 876w, 842m, 736s, 646w, 616w, 550m, 473m cm^{-1}. ESI-MS in MeCN: *m*/*z* 847.3 $(M + H)^+$. UV−vis in 6% DMF/Tris HCl buffer [λ_{max}, nm (ε, M^{-1} cm^{-1})]: 475 (5350), 380 nm (18 600), 362 (20 150), 270 (65 300). μ_{eff} (298 K): 5.91 μ_B.

The complexes were soluble in CH_2Cl_2, MeOH, EtOH, MeCN, DMF, and DMSO. They showed stability in solution, as evidenced from the mass spectral data showing the parent ion peak (Figures S1−S3, Supporting Information).

(38) Toshima, K.; Takano, R.; Ozawa, T.; Matsumura, S. *Chem. Commun.* **2002**, 212–213.
(39) Waring, M. J.; Fox, K. R. In *Molecular Aspects of Anti-cancer Drug Action*; Niedle, S., Waring, M. J., Eds.; MacMillan: New York, 1983; pp 127−156.
(40) Perrin, D. D.; Armarego, W. L. F.; Perrin, D. R. *Purification of Laboratory Chemicals*; Pergamon Press: Oxford, U. K., 1980.
(41) (a) Dickeson, J. E.; Summers, L. A. *Aust. J. Chem* **1970**, *23*, 1023–1027. (b) Collins, J. G.; Sleeman, A. D.; Aldrich-Wright, J. R.; Greguric, I.; Hambley, T. W. *Inorg. Chem.* **1998**, *37*, 3133–3141.
(42) Amouyal, E.; Homsi, A.; Chambron, J.-C.; Sauvage, J.-P. *J. Chem. Soc., Dalton Trans.* **1990**, 1841–1845.
(43) Wilson, J. G. *Aust. J. Chem.* **1990**, *43*, 1283–1289.
(44) Khan, O. *Molecular Magnetism*; VCH: Weinheim, Germany, 1993.

X-Ray Crystallographic Procedures. Diffraction data for **1**·EtOH·MeCN and **3**·MeOH·0.5EtOH·0.5MeCN were collected on a Bruker SMART APEX CCD diffractometer. Empirical absorption corrections were made using a multiscan program.[45] The structures were solved using the heavy-atom method and refined with full matrix least-squares using the SHELX system of programs.[46] The perspective views of the complexes were obtained using the ORTEP program.[47] Detailed crystallographic procedures are given as Supporting Information. Crystallographic details for **2**·MeCN were reported.[37] The structures refined well. The ethanol solvent molecule in **3**·MeOH·0.5EtOH·0.5MeCN showed disorder with two possible arrangements as CH_3CH_2OH and $HOCH_2CH_3$. A peak with an electron density of 1.017 was found near the central carbon atom of the ethanol molecule. The solvent molecules, however, did not show any apparent effect on the molecular structure of the complex.

DNA and Protein Binding Studies. DNA binding experiments were done with protein-free calf thymus DNA (250 μM NP) in a 5 mM Tris−HCl/NaCl buffer (pH 7.2) using a DMF solution of complexes **1**−**3**.[48] Absorption titration experiments were made using different concentrations of CT DNA, keeping the complex concentration constant for measuring the equilibrium binding constant (K_b) and the binding site size (*s*/b.p.) of the complex. The K_b values were determined from a nonlinear fitting of the plot of $\Delta\varepsilon_{af}/\Delta\varepsilon_{bf}$ versus [DNA] applying the McGhee−von Hippel (MvH) method and using the expression of Bard and co-workers (vide Supporting Information).[49,50] The apparent binding constant (K_{app}) values of complexes **1**−**3** were obtained with the fluorescence spectral technique using an EB-bound CT DNA solution in a Tris−HCl/NaCl buffer (pH 7.2; vide Supporting Information).[51−53] DNA thermal denaturation experiments were carried out by monitoring the absorbance of CT DNA (260 nm) at various temperatures in the absence and presence of the complexes in a 15:1 molar ratio of the CT DNA and the complex, with a ramp rate of 0.5 °C min^{-1} in a 5 mM phosphate buffer medium (pH 6.85) using a Cary 300 bio UV−visible spectrometer with a Cary temperature controller.

The protein binding studies were carried out by measuring the intrinsic fluorescence of BSA with increasing concentrations of complexes **1**−**3** as quenchers.[54] To the solutions of BSA (2 μM) in a phosphate buffer at pH 7.2 were added increments of the quencher, and the emission signals at 344 nm (excitation wavelength at 295 nm) were recorded after each addition of the quencher. F/F_0 versus [complex] plots were constructed, and the quenching constants were determined by linear fitting of the data according to the equation $F_0/F = 1 + K_{BSA}$[complex], where F_0 is the fluorescence intensity of BSA in the absence of the complex, F is the fluorescence intensity of BSA in the presence of the complex, K_{BSA} is the Stern Volmer quenching constant, and [complex] is the complex concentration.

DNA and Protein Cleavage Experiments. Photo-induced cleavage of pUC19 DNA by the ternary complexes **1**−**3** was carried out using a UV-A lamp (365 nm, 6W) or with visible light of a CW Argon−Krypton laser (50 mW power, Spectra Physics make, model Stabilite 2018-RM). The experiments were performed in a total volume of 18 μL containing SC DNA (1 μL, 33.3 μM), complex (2 μL) with varied concentrations, and a 50 mM Tris HCl buffer (pH 7.2) containing 50 mM NaCl. The samples were irradiated with UV-A or visible laser light, after which they were incubated for a further period of 1 h at 37 °C in the dark, followed by the addition of loading dye (25% bromophenol blue, 0.25% xylene cyanol and 30% glycerol (3 μL)), and finally loaded on a 1% agarose gel containing 1 μg mL^{-1} of EB. The gels were run at 45 V for 2 h in a TAE buffer, and the DNA bands were visualized using UV light, photographed, and the intensities of the bands quantified using the UVITECH Gel Documentation System. Due corrections were made for the small amount of nicked circular (NC) form present in the original SC DNA and the higher affinity of EB for NC and linear forms over the SC form.[55] The error in measuring the band intensities varied from 3 to 5%. For the inhibition studies, the reagent (DMSO, 4 μL; KI, 0.5 mM; TEMP, 0.5 mM; DABCO, 0.5 mM; catalase, 4 units; superoxide dismutase, 4 units; distamycin-A, 50 μM) was added to SC DNA prior to the addition of the complexes. For D_2O experiments, this solvent was used for dilution to 18 μL. Detailed experimental procedures are given as Supporting Information. Photochemical protein cleavage experiments were carried out according to the standard procedures using BSA (15 μM) dissolved in a 50 mM Tris−HCl buffer (pH, 7.2) photoirradiated in the presence of different concentrations of **3** at 365 nm (6W) for 2 h, followed by SDS PAGE with Coomassie Brilliant Blue R-250 for staining.[56,57]

Cell Cytotoxicity Assay. The phototoxicities of the complexes were assessed using the 3-(4,5-dimethylthiazol-2-yl)-2,5-diphenyltetrazolium bromide (MTT) assay based on the ability of mitochondrial dehydrogenases in the viable cells to cleave the tetrazolium rings of MTT, forming dark blue membrane impermeable crystals of formazan that can be quantified at 595 nm on detergent solubulization.[58] The level of the formazan product formed is a measure of the number of viable cells. Approximately, 8000 cells of human cervical carcinoma (HeLa) and human keratinocytes (HaCaT) were plated in a 96-well culture plate in DMEM containing either 10% FBS (for HeLa) or 10% heat-inactivated FBS (for HaCaT). After 24 h of incubation at 37 °C in a CO_2 incubator, different concentrations of the iron complexes or cisplatin dissolved in 1% DMSO were added to the cells, and incubation was continued for 4 h in the dark. After incubation, the medium was replaced with PBS and photoirradiated with UV-A (365 nm) light (fluence rate: 610 μW cm^{-2} for 15 min) or filtered (400−700 nm) visible light from a 300 W tungsten lamp (fluence rate: 6.8 mW cm^{-2}) to provide a total dose of 20 *J* cm^{-2}. Post irradiation, PBS was replaced with DMEM-FBS, and incubation was continued for a further 12 h in the dark. At the end of this incubation, 20 μL of 5 mg mL^{-1} of MTT was added to each well and incubated for an additional 3 h. The culture medium was discarded, and 200 μL of DMSO was added to dissolve the formazan crystals. The abosorbance at 595 nm was determined using a BIORAD ELISA plate reader. The cytotoxicity of the test compounds was measured as the percentage ratio of the absorbance

(45) Walker, N.; Stuart, D. *Acta Crystallogr.* **1993**, *A39*, 158–166.
(46) Sheldrick, G. M. *SHELX-97*; University of Göttingen: Göttingen, Germany, 1997.
(47) Johnson, C. K. *ORTEP, Report ORNL-5138*; Oak Ridge National Laboratory: Oak Ridge, TN, 1976.
(48) Reichman, M. E.; Rice, S. A.; Thomas, C. A.; Doty, P. *J. Am. Chem. Soc.* **1954**, *76*, 3047–3053.
(49) McGhee, J. D.; von Hippel, P. H. *J. Mol. Biol.* **1974**, *86*, 469–489.
(50) Carter, M. T.; Rodriguez, M.; Bard, A. J. *J. Am. Chem. Soc.* **1989**, *111*, 8901–8911.
(51) Waring, M. *J. Mol. Biol.* **1965**, *13*, 269–282.
(52) LePecq, J.-B.; Paoletti, C. *J. Mol. Biol.* **1967**, *27*, 87–106.
(53) Lee, M.; Rhodes, A. L.; Wyatt, M. D.; Forrow, S.; Hartley, J. A. *Biochemistry* **1993**, *32*, 4237–4245.
(54) Quiming, N. S.; Vergel, R. B.; Nicolas, M. G.; Villanueva, J. A. *J. Health Sci.* **2005**, *51*, 8–15.
(55) Bernadou, J.; Pratviel, G.; Bennis, F.; Girardet, M.; Meunier, B. *Biochemistry* **1989**, *28*, 7268–7275.
(56) Kumar, C. V.; Buranaprapuk, A.; Sze, H. C.; Jockusch, S.; Turro, N. J. *Proc. Natl. Acad. Sci. U. S. A.* **2002**, *99*, 5810–5815.
(57) Schägger, H.; von Jagow, G. *Anal. Biochem.* **1987**, *166*, 368–379.
(58) Mosmann, T. *J. Immunol. Methods* **1983**, *65*, 55–63.

of the treated cells to the untreated controls. The IC_{50} values were determined by nonlinear regression analysis (GraphPad Prism).

Nuclear Staining. The changes in chromatin organization following photoexposure after treatment with **3** were determined microscopically by assessing staining with Hoechst 33258 and an acridine orange/ethidium bromide (AO/EB) dual stain. Hoechst staining was performed as described by Lee and Shacter.[59] Briefly, the control and the cells treated with **3** (10 μM) for 4 h in the dark, followed by irradiation with visible light of 400−700 nm (20 *J* cm^{-2}), were fixed with 3.7% (v/v) paraformaldehyde in PBS for 10 min at room temperature, permeabilized with 0.1% Triton X-100 for 10 min, and stained with Hoechst 33258 (1 mg mL^{-1} in PBS) for 5 min. After being washed twice with PBS, cells were examined by fluorescence microscopy (360/40 nm excitation and 460/50 nm emission filters). The apoptotic cells were identified by the presence of highly condensed or fragmented nuclei. The protocol for AO/EB that was used was derived from the reported ones.[60] HeLa cells cultured on 35 mm culture dishes were photoirradiated with visible light (400−700 nm, 20 *J* cm^{-2}) following 4 h of incubation in the dark in the presence of 10 μM **3**. The cells were then allowed to recover for 1 h or washed thrice with PBS and stained with an AO/EB mixture (1:1, 10 μM) for 15 min and observed at 10× magnification with a fluorescence microscope using 485/20 nm excitation and 535/40 nm emission filter sets.

Measurement of Reactive Oxygen Species (ROS). The measurement of the intracellular ROS was based on the oxidation of DCFH-DA, a nonpolar molecule capable of penetrating the cell membrane, which first gets hydrolyzed by the cellular esterases to 2′,7′-dichlorodihydrofluorescein (DCFH), which in turn is oxidized to the fluorophore dichlorofluorescein (DCF).[61] The HeLa cells treated with **3** or the appropriate controls, after photoirradiation with visible light (400−700 nm, 20 *J* cm^{-2}), were washed twice with PBS, incubated with 10 μM DCFH-DA in PBS for 20 min, washed, and overlaid with a DMEM/10% FBS medium under strictly dark conditions to avoid any nonspecific artifacts.[62] DCF levels were assessed by fluorescence microscopy directly after sample processing, using 485/20 nm excitation and 535/40 nm emission filter sets. The quantitative assessment of the ROS levels was carried out by fluorimetric analysis using the protocol described by Stadtman and co-workers.[63]

Alkaline Single-Cell Gel Electrophoresis (Comet Assay). An alkaline comet assay was performed to measure the extent of DNA fragmentation induced by **3** (20 μM) in the HeLa cells 2 h after exposure to the visible light (400−700 nm, 20 *J* cm^{-2}).[64,65] Briefly, 1×10^4 mL^{-1} of treated and untreated HeLa cells was mixed with 0.5% low-melting-point agarose at a ratio of 1:10 (v/v) and spread on slides precoated with 1% normal agarose. The embedded cells were lysed in a precooled lytic solution (2.5 M NaCl, 100 mM EDTA, 10 mM Tris base and 1% Triton X-100, pH 10) at 4 °C for 60 min, rinsed, and equilibrated in an alkaline electrophoresis buffer (0.3 M NaOH and 1 mM EDTA). Electrophoresis was performed at 1.0 V cm^{-1} for 30 min, and the slides were neutralized with 0.4 M Tris (pH 7.5) stained with EB solution (2 μg mL^{-1}) and analyzed using a fluorescence microscope equipped with 540/25 excitation and 605/55 emission filter sets. The DNA contents in the head and tail were quantified using "Comet score" from Autocomet.

Caspase 3/7 Activity. Caspase 3/7 activity was measured according to the literature procedure.[66] For determination of caspase 3/7 activity, the cells plated in 35 mm culture dishes were incubated with different concentrations of **3** (20, 40, and 100 μM) for 4 h in the dark followed by irradiation with visible light (400−700 nm, 20 *J* cm^{-2}) in PBS. For determining the nonspecific protease activity, the general caspase inhibitor Z-Val-Ala-Asp-fluoromethylketone (ZVAD-FMK; 10 μM; Promega) was added prior to photoexposure. The cells were lysed 2 h post photoexposure in a lysis buffer containing 1% Nonidet P-40 detergent; 20 mM Tris−HCl, pH 8.0; 137 mM NaCl; 10% glycerol supplemented with 1 mM PMSF; aprotinin (0.15 U mL^{-1}); and 1 mM sodium orthovanadate for 20 min on ice. The lysates were centrifuged for 10 min at 16 000*g* at 4 °C, and 100 μg of the protein of the lysate supernatants was incubated in the assay buffer (1% NP-40; 20 mM Tris−HCl, pH 7.5; 137 mM NaCl; 10% glycerol) with 100 μM of acetyl-Asp-Glu-Val-Asp-amido-4-methylcoumarin at 37 °C for 2 h. The reactions were terminated on adding double-distilled ethanol, and AMC released was determined by measuring the fluorescence with a Perkin-Elmer LS-50B luminescence spectrometer with excitation at 360 nm and emission at 440 nm.

Results and Discussion

Synthesis and General Aspects. Ternary iron(III) complexes [FeL(B)] (**1**−**3**) were synthesized in good yields from the reaction of $Fe(NO_3)_3 \cdot 9H_2O$ with a trianionic tetradentate ligand (H_3L) and the phenanthroline base (B: phen, **1**; dpq, **2**; dppz, **3**). The choice of the tetradentate ligand H_3L with two phenolate, one amine, and one acetate O-donor site is based on its ability to stabilize the iron(III) redox state in the presence of intracellular reducing agents like glutathione and to impart higher lipophilic character in the presence of *tert*-butyl groups for better cellular uptake.[67] In addition, the phenolate ligands are known to show low-energy ligand-to-iron(III) charge transfer electronic transition.[68] We have chosen planar phenanthroline bases due to their DNA binding propensity. In addition, the dpq and dppz ligands with quinoxaline and phenazine moieties could act as photosensitizers.[38] Complexes **1**−**3** were characterized from analytical, spectral, and X-ray crystallographic studies (Tables 1 and 2).

All of the complexes are discrete monomeric nonelectrolytic in solution and do not have any labile ligands, as evidenced from the molar conductance and mass spectral data. The electronic spectra of the complexes in a 50 mM Tris−HCl buffer containing 6% DMF (pH 7.2) display a broad phenolate-to-Fe(III) charge transfer band near 500 nm. This band extends down to the PDT spectral window, thus allowing us to explore the photoinduced DNA cleavage

(59) Lee, Y. J.; Shacter, E. *J. Biol. Chem.* **1999**, *274*, 19792–19798.
(60) Coligan, J. E.; Kruisbeck, A. M.; Margulies, D. H.; Shevach, E. M.; Strober, W. In *Related Isolation Procedures and Functional Assay, Current Protocols in Immunology*; Coico, R., Ed.; John Wiley & Sons, Inc.; New York, 1995, p 3.17.1.
(61) Le Bel, C. P.; Ischiropoulos, H.; Bondy, S. C. *Chem. Res. Toxicol.* **1992**, *5*, 227–231.
(62) Bilski, P.; Belanger, A. G.; Chignell, C. F. *Free Radical Biol. Med.* **2002**, *33*, 938–946.
(63) Oubrahim, H.; Stadtman, E. R.; Chock, P. B. *Proc. Natl. Acad. Sci. U. S. A.* **2001**, *98*, 9505–9510.
(64) Singh, N. P.; McCoy, M. T.; Tice, R. R.; Schneider, E. L. *Exp. Cell Res.* **1988**, *175*, 184–191.
(65) David, O.; Bourré, L.; Krika, Y.; Durand, M.; Patrice, T. *Photodiag. Photodyn. Ther.* **2005**, *2*, 25–33.
(66) (a) Granville, D. J.; Levy, J. G.; Hunt, D. W. *Cell Death Differ.* **1997**, *4*, 623–629. (b) Pareek, T. K.; Joshi, A. R.; Sanyal, A.; Dighe, R. R. *Apoptosis* **2007**, *12*, 1085–1100.
(67) (a) Drain, C. M.; Christensen, B.; Mauzerall, D. C. *Proc. Natl. Acad. Sci. U. S. A.* **1989**, *86*, 6959–6962. (b) Drain, C. M.; Mauzerall, D. C. *Biophys. J.* **1992**, *63*, 1556–1563.
(68) Shongwe, M. S.; Kaschula, C. H.; Adsetts, M. S.; Ainscough, E. W.; Brodie, A. M.; Morris, M. J. *Inorg. Chem.* **2005**, *44*, 3070–3079.

Table 1. Selected Crystallographic Data for the Complexes **1** and **3**

	1·MeCN·EtOH	**3**·0.5MeCN·0.5EtOH·MeOH
empirical formula	$C_{48}H_{63}FeN_4O_5$	$C_{53}H_{64.5}FeN_{5.5}O_{5.5}$
fw	831.87	922.45
crystal system	triclinic	triclinic
space group	$P\bar{1}$	$P\bar{1}$
unit cell dimensions:		
a, Å	9.657(3)	14.887(3)
b, Å	14.179(4)	15.120(3)
c, Å	18.778(5)	25.123(5)
α, deg	104.387(5)	74.456(4)
β, deg	102.537(6)	75.996(4)
γ, deg	103.424(5)	65.834(4)
V, Å^3	2317.2(12)	4914.1(17)
Z	2	4
T, K	293(2)	293(2)
ρ_{calcd}, g cm^{-3}	1.192	1.247
λ, Å (Mo Kα)	0.71073	0.71073
μ, cm^{-1}	3.82	3.60
data/restraints/params	8140/0/535	17247/2/991
F(000)	860	1964
goodness-of-fit	1.053	1.019
R (F_o)[a], $I > 2\sigma(I)$/wR (F_o)[b]	0.0647/0.1548	0.0955/0.2377
R (all data)/wR (all data)	0.1055/0.1768	0.1516/0.2758
largest diff. peak and hole (e Å^{-3})	0.813, −0.252	1.017, −0.886

[a] $R = \sum||F_o| - |F_c||/\sum|F_o|$. [b] $wR = \{\sum[w(F_o^2 - F_c^2)^2]/\sum[w(F_o)^2]\}^{1/2}$. $w = [\sigma^2(F_o)^2 + (AP)^2 + BP]^{-1}$, where $P = (F_o^2 + 2F_c^2)/3$, $A = 0.1377$ and $B = 0.6093$ for **1**·MeCN·EtOH, and $A = 0.1189$ and $B = 9.2533$ for **3**·0.5MeCN·0.5EtOH·MeOH.

activity of the complexes in red light (Figure 1, Figure S4 in the Supporting Information). The spectral pattern and the band intensities remain unaltered on keeping the solution for a long time, suggesting the stability of the coordination geometry in the complexes (Figure S5 in the Supporting Information). Magnetic susceptibility measurements on the solid samples of the complexes at 25 °C show the high-spin nature of the 3d^5-iron(III), giving magnetic moment values of ∼5.9 μ_B. The complexes are redox-active, showing an Fe(III)−Fe(II) couple near −0.6 V (ΔE_p, 80−100 mV at 50 mV s^{-1}) versus SCE in DMF−0.1 M TBAP (Figure 1).[37] Complex **1** shows only a cathodic response at −0.62 V versus SCE without any anodic counterpart (Figure S6, Supporting Information). The redox potential of −0.6 V makes the ferric state stable in the complexes. Complex **3**, in addition, displays a quasi-reversible voltammogram at −1.09 V versus SCE ($\Delta E_p = 82$ mV) due to dppz reduction.

The ternary iron(III) complexes are structurally characterized by the single-crystal X-ray diffraction technique. The crystal structure of complex **2** was reported earlier by us.[37] Complexes **1** and **3** crystallized in the same $P\bar{1}$ space group belonging to the triclinic crystal system. Complex **2** crystallizes in the monoclinic $P2_1/n$ space group. An ORTEP view of one molecule of **3** in the crystallographic asymmetric unit is shown in Figure 2. Selected bond distances and angles are given in Tables S1 and S2 (Supporting Information). ORTEP views of the phen (**1**) and two molecules of the dppz (**3**) complexes along with the unit cell packing diagrams are shown in Figures S7−S10 (vide Supporting Information). All three complexes are discrete mononuclear with the iron(III) center in a six-coordinate FeO_3N_3 coordination geometry. The trianionic ligand L shows the tetradentate mode of bonding, while the phenanthroline bases are bidentate chelating in nature. The Fe−O and Fe−N distances are in the ranges 1.891(2)−2.041(3) Å and 2.148(3)−2.375(3) Å, respectively. One of the Fe−N(phenanthroline base) distances is significantly longer (2.354 Å) than the other Fe−N(phenanthroline base) distance (2.168 Å). This may be due to the trans influence of the phenolate oxygen atom showing an Fe−O distance of 1.899 Å. The molecular structures of the complexes in the solid state are in agreement with the mass spectral data in solution showing the stability of the structures in both the solid and solution phases.

DNA Binding Studies. The binding propensity of the Fe(III) complexes **1**−**3** to CT DNA has been studied using various techniques. Selected data are given in Table 2. Absorption spectral measurements have been carried out to determine the equilibrium binding constant (K_b) and binding site size (*s*/b.p.) of the complexes to CT-DNA by monitoring the change in the absorption intensity of the spectral band at 266 nm for **1** and **2** and at 270 nm for complex **3**. The complexes show minor bathochromic shifts of ∼2−6 nm of the spectral band, suggesting groove binding preference (Figure 3, Figure S11 in Supporting Information). The K_b and *s* values of **1**−**3** are in the range of 8.0×10^4 to 3.2×10^5 M^{-1} and 0.1−0.7, respectively. Complex **3**, having a dipyridophenazine ligand with an extended planar phenazine moiety, shows the highest binding propensity to CT-DNA. The *s* value that is obtained from the theoretical fit gives a measure of the number of DNA bases associated with the complex.[69] The low value of *s* indicates a DNA groove-binding nature of the complexes in preference to intercalation due to the presence of steric bulk of the ancillary tetradentate ligand, having bulky *tert*-butyl groups. A low value of s (≤ 1) could also be due to an aggregation of hydrophobic molecules on the DNA surface by π stacking. The dpq and dppz ligand with its respective extended quinoxaline and phenazine aromatic rings can undergo partial π-stacking interactions with the purine and pyrimidine DNA bases. The DNA binding propensity of the complexes is also determined from the competitive ethidium bromide displacement assay using the fluorescence spectral method, giving K_{app} values of the order: **3** (dppz) > **2** (dpq) > **1** (phen) (Figure S12 in the Supporting Information). DNA thermal denaturation experiments show only a minor shift in the DNA melting temperature (T_m), giving ΔT_m values of 1−3 °C on addition of the complexes to CT- DNA (Figure 4). The data suggest a primarily groove-binding nature of the complexes. Intercalating ligands like EB show significantly high ΔT_m values.[70]

DNA Photocleavage Activity. The photoinduced DNA cleavage activity of the ternary Fe(III) complexes has been studied using SC pUC19 DNA (33.3 μM, 0.2 μg) in a medium of Tris−HCl/NaCl (50 mM, pH 7.2) buffer on irradiation with a low-power monochromatic UV-A light of 365 nm (6W) and visible light of wavelengths 476, 514, 532, 568, and 647 nm (50 mW) using a CW argon−krypton

(69) Nair, R. B.; Teng, E. S.; Kirkland, S. L.; Murphy, C. J. *Inorg. Chem.* **1998**, *37*, 139–141.
(70) Chouai, A.; Wicke, S. E.; Turro, C.; Bacsa, J.; Dunbar, K. R.; Wang, D.; Thummel, R. P. *Inorg. Chem.* **2005**, *44*, 5996–6003.

Table 2. Selected Physicochemical Data for the Complexes **1**−**3**

complex	IR[a]/ cm^{-1}, ν(C═O)	λ, nm (ε, M^{-1} cm^{-1})[b]	Λ_M[c]/ S m^2 M^{-1}	$E_{1/2}$/V (ΔE_p, mV)[d]	μ_{eff}[e]	ΔT_m[f]/°C	K_b/M^{-1} (*s*/b.p.)[g]	K_{app}[h]/M^{-1}	K_{BSA}[i]/M^{-1}
[FeL(phen)] (**1**)	1660	490 (5,150)	12	0.62[j]	5.85	1.2	8.8(±1.7) × 10^4 [0.1]	1.2 × 10^5	8.4 × 10^4
[FeL(dpq)] (**2**)[k]	1670	470 (5,140)	10	0.62 (95)	5.86	2.1	2.1(±0.6) × 10^5 [0.7]	3.3 × 10^5	1.3 × 10^5
[FeL(dppz)] (**3**)	1667	475 (5,340)	16	0.61 (98)	5.91	3.0	3.2(±0.9) × 10^5 [0.4]	5.7 × 10^5	1.1 × 10^5

[a] In KBr phase. [b] Visible electronic bands in a 6% DMF−Tris-HCl buffer. [c] Λ_M, molar conductance in DMF at 25 °C. [d] Scan rate of 50 mV s^{-1} in DMF−0.1 M TBAP. Potentials are vs a SCE. $E_{1/2} = 0.5(E_{pa} + E_{pc})$. $\Delta E_p = (E_{pa} - E_{pc})$, where E_{pa} and E_{pc} are anodic and cathodic peak potentials, respectively. [e] μ_{eff} in μ_B for solid powdered samples at 298 K. [f] Change in the DNA melting temperature. [g] K_b, DNA binding constant (*s*, binding site size). [h] K_{app}, apparent DNA binding constant. [i] K_{BSA}, Stern−Volmer quenching constant for BSA fluorescence. [j] The value corresponds to E_{pc} with no anodic counterpart. [k] Ref 37.

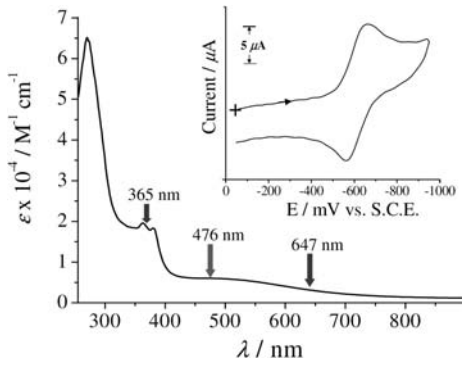

Figure 1. Electronic absorption spectrum of complex **3** in a DMF−Tris HCl buffer with arrows showing selected wavelengths used for DNA photocleavage studies. The inset shows the cyclic voltammogram of complex **3** in DMF−0.1 M TBAP at a scan rate of 50 mV s^{-1}.

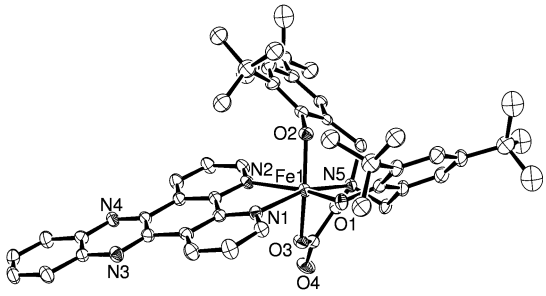

Figure 2. An ORTEP view of [FeL(dppz)] (**3**) showing 30% probability thermal ellipsoids of one of the two independent molecules in the asymmetric unit of the $P\bar{1}$ space group. The hydrogen atoms and solvent molecules are removed for clarity.

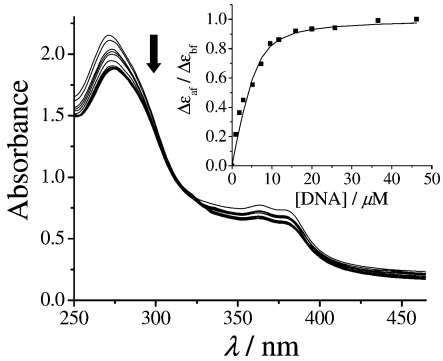

Figure 3. Absorption spectral traces of complex **3** in a 5 mM Tris−HCl buffer (pH 7.2) on increasing the quantity of CT DNA. The inset shows the least-squares fit of $\Delta\varepsilon_{af}/\Delta\varepsilon_{bf}$ vs [DNA] for complex **3** (■) using the MvH equation (vide Supporting Information).

mixed gas ion laser. The gel electrophoresis diagrams showing the extent of DNA cleavage from SC to the NC form are shown in Figures 5 and 6 (514, 532, and 568 nm data are in Figures S13 and S14 in the Supporting Information). Selected DNA cleavage data are given in Table 3. The

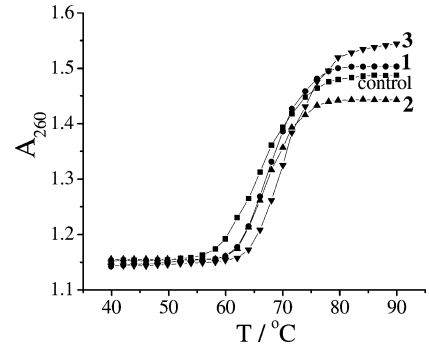

Figure 4. Thermal denaturation profiles of 150 μM NP CT DNA between 40 and 90 °C without any complex (■) and in the presence of 10 μM of **1** (●), **2** (▲), and **3** (▼).

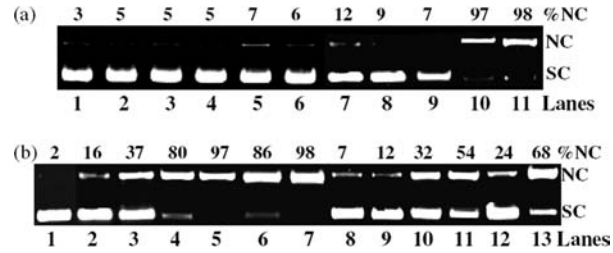

Figure 5. (a) Cleavage of SC pUC19 DNA (0.2 μg, 33.3 μM) by [FeL(B)] (5.6 μM; B = phen, **1**; dpq, **2**; dppz, **3**) in a Tris−HCl/NaCl buffer (pH 7.2) containing 10% DMF on photoexposure to UV-A light of 365 nm (6 W) for 2 h: lane 1, DNA control; lane 2, DNA + $Fe(NO_3)_3 \cdot 9H_2O$ (33.3 μM); lane 3, DNA + H_3L (33.3 μM); lane 4, DNA + dpq (33.3 μM); lane 5, DNA + dppz (33.3 μM); lanes 6−8, DNA + complexes **1**−**3** (2 h incubation in dark with no photoexposure); lanes 9−11, DNA + complexes **1**−**3**. (b) Cleavage of SC pUC19 DNA (0.2 μg, 33.3 μM) by [FeL(B)] (33.3 μM; B = phen, **1**; dpq, **2**; dppz, **3**) in a Tris−HCl/NaCl buffer (pH 7.2) containing 10% DMF in visible light of 476 and 647 nm (50 mW; exposure time (*t*), h): lane 1, DNA control (476 nm, 2 h); lane 2, DNA + **1** (476 nm, 1 h); lane 3, DNA + **1** (476 nm, 2 h); lane 4, DNA + **2** (476 nm, 1 h); lane 5, DNA + **2** (476 nm, 2 h); lane 6, DNA + **3** (476 nm, 1 h); lane 7, DNA + **3** (476 nm, 2 h); lane 8, DNA + **1** (647 nm, 1 h); lane 9, DNA + **1** (647 nm, 2 h); lane 10, DNA + **2** (647 nm, 1 h); lane 11, DNA + **2** (647 nm, 2 h); lane 12, DNA + **3** (647 nm, 1 h); lane 13, DNA + **3** (647 nm, 2 h).

cleavage activity at 365 nm follows the order: **3** (dppz) > **2** (dpq) ≫ **1** (phen) (Figure 5a). A 5.5 μM concentration of the complexes **2** and **3** shows essentially complete cleavage of the SC DNA for an exposure time of 2 h (Figure 5a, lanes: 10, 11). Complex **1** containing phen is photo-inactive at this wavelength. The UV-A light-induced DNA cleavage is likely to involve photoactivation of the dpq and dppz ligands having quinoxaline and phenazine moieties with conjugated C═N bonds that could generate photoexcited $^3(n-\pi^*)$ and $^3(\pi-\pi^*)$ state(s).[38] Control experiments with $Fe(NO_3)_2 \cdot 9H_2O$ (33.3 μM) and the ligands H_3L, phen, dpq, and dppz (33.3 μM) alone do not show any significant photocleavage of DNA at 365 nm. Dark controls with complexes **1**−**3** are also ineffective at causing any DNA damage. Photolysis of SC

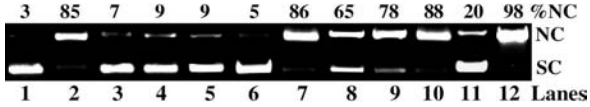

Figure 6. Mechanistic aspects of the photocleavage of SC pUC19 DNA (0.2 μg, 33.3 μM) by complex **3** (33.3 μM) in a 50 mM Tris−HCl/NaCl buffer (pH, 7.2) containing 10% DMF on photoirradiation at 476 nm (50 mW) for 2 h in the presence of different additives: lane 1, DNA control; lane 2, DNA + **3**; lane 3, DNA + KI (500 μM) + **3**; lane 4, DNA + DMSO (4 μL) + **3**; lane 5, DNA + SOD (4 units) + **3**; lane 6, DNA + catalase (4 units) + **3**; lane 7, DNA + TEMP (500 μM) + **3**; lane 8, DNA + NaN_3 (500 μM) + **3**; lane 9, DNA + DABCO (500 μM) + **3**; lane 10, DNA + L-histidine (500 μM) + **3**; lane 11, DNA + distamycin-A (50 μM); lane 12, DNA + distamycin-A (50 μM) + **3** [complexes **1** and **2** showed 21% and 24% NC form, respectively, in the distamycin-A experiments under similar conditions].

Table 3. Photoinduced SC DNA (0.2 μg, 33.3 μM) Cleavage Data[a]

Sl. no.	reaction condition	[complex]: 365 nm [647 nm]/μM	t/min	$\%NC_{365nm}$ [$\%NC_{647\ nm}$]
1	DNA control		2 h	3 [2]
2	DNA + [FeL(dppz)] (**3**) (in dark)	5.6 [33.3]	2 h	5 [7]
3	DNA + [FeL(phen)] (**1**)	5.6 [33.3]	2 h	7 [12]
4	DNA + [FeL(dpq)] (**2**)	5.6 [33.3]	2 h	97 [54]
5	DNA + [FeL(dppz)] (**3**)	5.6 [33.3]	2 h	98 [68]

[a] SC and NC are the supercoiled and nicked circular forms of pUC19 DNA, respectively. The error in measuring %DNA is 3−5%. t, exposure time. Light sources: UV light (365 nm, 6 W) and visible light [Ar−Kr CW laser (647 nm, 50 mW)].

DNA in the presence of the complexes (33.3 μM) at visible wavelengths of 476, 514, 532, 568, and 647 nm from a tunable CW Ar−Kr laser (50 mW laser power) shows efficient photocleavage of DNA by the dpq and dppz complexes (Figure 5b, Figures S13 and S14 in the Supporting Information). The notion behind the study using different wavelengths is based on the observation of an absorption tail that extends down into the PDT spectral window (>600 nm). We previously reported the DNA cleavage activity of [FeL(dpq)] (**2**) in UV-A and red light.[37] Complex **3**, having dppz, shows better DNA photocleavage activity than **2** in red light. The extent of DNA cleavage follows the spectral pattern as the extinction coefficient of the iron(III)−phenolate charge-transfer band decreases on increasing the wavelength.

The mechanistic aspects of the photoinduced DNA cleavage activity of the complexes **1**−**3** have been investigated using various additives at UV-A and visible wavelengths (476 and 647 nm; Figure 6, Figure S15 in the Supporting Information). The addition of singlet oxygen quenchers DABCO, TEMP, sodium azide, and L-histidine shows no inhibitory effect on the DNA cleavage activity at 365 and 476 nm for complexes **2** and **3**. Hydroxyl radical scavengers like DMSO and KI, however, display significant reduction in the DNA cleavage activity at these wavelengths. Hydrogen peroxide and superoxide scavengers like catalase and SOD show inhibition of the DNA cleavage activity. The results suggest the involvement of hydroxyl radicals ($HO^{\bullet}$) in the photocleavage reaction in both UV-A and visible light. The involvement of singlet oxygen ($^1O_2$) is also ruled out since there is no enhancement in the DNA cleavage activity in the presence of D_2O.[71] We have studied the groove-binding preference of the complexes using DNA minor groove-binder

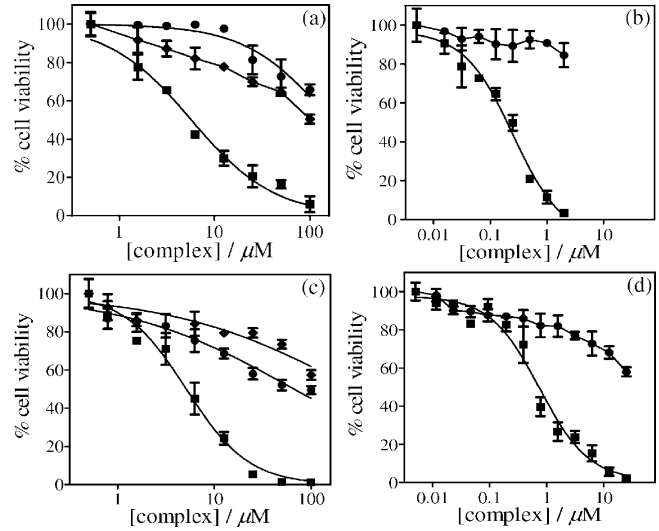

Figure 7. Photocytotoxicity of complex **3**: (a) effect of visible light exposure (400−700 nm, 20 J cm^{-2}) on HeLa cells, (b) effect of UV-A light exposure (365 nm, 610 μW cm^{-2} for 15 min) on HeLa cells, (c) effect of visible light exposure (400−700 nm, 20 J cm^{-2}) on human keratinocytes HaCaT cells, and (d) effect of UV-A light exposure (365 nm, 610 μW cm^{-2} for 15 min) on human keratinocyte HaCaT cells. The squares (■) denote irradiated cells, and circles (●) represent dark controls. Cisplatin-treated cells are shown by ◆.

distamycin-A, which alone shows ∼25% cleavage of the SC DNA at 365 nm for an exposure time of 2 h. The addition of complex **2** (5.5 μM) to distamycin-A bound DNA shows no significant increase in the DNA cleavage activity, suggesting minor groove-binding propensity of **2**.[37] The DNA cleavage activity of **3** remains unaffected in the presence of distamycin-A, indicating major groove-binding preference of the dppz complex. The DNA cleavage activity has also been studied under an anaerobic medium using argon. The complexes do not show any DNA photocleavage activity under argon. The visible light mechanistic data suggest a photoredox pathway in which the metal could get reduced on photoactivation of the LMCT band, forming a charge-separated $Fe^{2+}-L^{\bullet+}$(phenolate ligand radical cation) as the reactive species that possibly reduces O_2 to $O_2^{\bullet-}$ by the reactive Fe^{2+} ion with subsequent formation of hydroxyl radicals in the reaction $3O_2^{\bullet-} + 2H^+ \rightarrow HO^{\bullet} + HO^- + 2O_2$, as reported for the antitumor natural product podophyllotoxin (Scheme S1, Supporting Information).[72] EPR spectral measurements on **2** using 5,5-dimethyl-1-pyrroline *N*-oxide (DMPO) show DMPO−$HO^{\bullet}$ formation (Figure S16a in Supporting Information). Photoactivation of the dpq complex **2** under argon shows significant reduction of the phenolate-to-iron(III) charge transfer band intensity that reverts back on exposure to O_2 (Figure S16b in Supporting Information). The mechanistic pathway in UV-A light could have a similar photoredox pathway, forming a reactive $Fe^{2+}-B^{\bullet+}$ intermediate involving the photo- and redox-active dpq and dppz bases.[20]

Interaction with Serum Protein. Small molecule−serum protein interaction is an important aspect of metal-based drug metabolism. Such interactions are capable of affecting the

(71) Khan, A. U. *J. Phys. Chem.* **1976**, *80*, 2219–2227.

(72) Sakurai, H.; Miki, T.; Imakura, Y.; Shibuya, M.; Lee, K.-H. *Mol. Pharmacol.* **1991**, *40*, 965–973.

Table 4. IC_{50} values of Complex **3**, Cisplatin, and Photofrin in HeLa and HaCaT Cell Lines

	HeLa			HaCaT		
complex	IC_{50} (μM) dark	IC_{50} (μM) UV-A	IC_{50} (μM) visible	IC_{50} (μM) dark	IC_{50} (μM) UV-A	IC_{50} (μM) visible
[FeL(dppz)] (**3**)[a]	>100	0.25 ± 0.13	3.59 ± 1.2	>100	0.75 ± 0.24	6.07 ± 2.2
Photofrin[b]	>41[c]		4.28 ± 0.2[c]			
Cisplatin[d]	24[e]			173[f]	144[f]	

[a] The dpq complex **2** did not show any cytotoxicity in the dark or upon photoirradiation with either UV-A or visible light. [b] The Photofrin values are taken from ref 7 (converted to μM using the approximate molecular weight of Photofrin, 600 g mol^{-1}). [c] At 633 nm excitation (fluence rate: 5 *J* cm^{-2}). The UV-A light of wavelength 365 nm (610 μW cm^{-2}). Visible light: 400−700 nm, 6.8 mW cm^{-2}. [d] The IC_{50} values are taken from ref 23b. Cisplatin IC_{50} values were outside the concentration range (100 μM) used in our studies. [e] The IC_{50} values were expressed in μg mL^{-1} and converted to μM for comparison. [f] The IC_{50} values (with fluence rate of 5 *J* cm^{-2} of UV) are taken from ref 30.

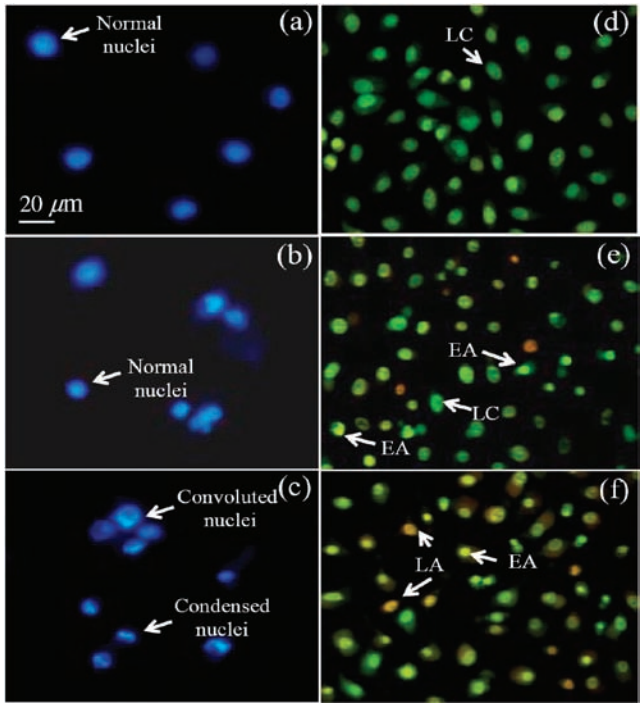

Figure 8. (a−c) Hoechst 33258 staining of complex **3** untreated and treated HeLa cells permeabilized with TBST and fixed with paraformaldehyde (3.7%) 2 h after photoexposure to identify nuclear morphology: (a) untreated cells, (b) only light-treated controls, and (c) treated with complex **3** and exposed to visible light (20 *J* cm^{-2}). (d−f) Acridine orange/ethidium bromide dual staining of HeLa cells to identify live (LC), early apoptotic (EA), and late apoptotic (LA) nuclei: (d) untreated control (only light), (e) 1 h after photoexposure with complex **3** and visible light (20 *J* cm^{-2}), and (f) 2 h after photoexposure with complex **3** and visible light (20 *J* cm^{-2}).

distribution and biotransformation, and ultimately the mechanism of action, of the medicinal agent.[73] The ability of the ternary Fe(III) complexes to interact with the serum protein, namely, BSA, has been investigated by tryptophan emission-quenching experiments in the presence of complexes **1**−**3**. The fluorescence intensity of BSA is known to be dependent upon the degree of exposure of two tryptophan side chains, 134 and 212, to the immediate polar surroundings and to quenching groups like protonated carbonyl, protonated imidazole, and tyrosinate anions.[74−76] The emission intensity of BSA has been found to decrease with a gradual increase in the concentration of complexes **1**−**3**, possibly due to changes in the secondary structure of BSA, leading to exposure of one or both of the tryptophan residues of BSA (Figure S17a in the Supporting Information). This decrease in emission intensity may be attributed to the hydrophobic interaction of the complexes through its *tert*-butyl groups with BSA (Table 2).[77] This is also highlighted from the fact that the complexes display nearly similar binding affinity to BSA (K_{BSA} ~1.0×10^5 M^{-1}). The ability of complex **3** to photocleave BSA on 365 nm photoirradiation has been studied, and the products were analyzed by 12.5% SDS-PAGE. The complex is cleavage-inactive in the concentration range of 25−100 μM used for the study. Complex **3** seems to act more as a potent photonucleolytic agent rather than being a photochemical protein scissor. The Coomassie-stained SDS-PAGE gel is shown in Figure S17b in the Supporting Information.

Cytotoxicity Study. To test the ability of complexes **2** and **3** to inhibit growth and induce cell death upon photoexcitation with UV-A or visible light in HeLa and HaCaT cell lines, an MTT assay was performed (Figure 7, Figure S18 in Supporting Information). The HeLa cells were used as a highly proliferative human cancer model, whereas the HaCaT cells represent a model system of proliferating keratinocytes for topical application of PDT in nonmalignant skin disorders. Complex **3** caused a reduction in the viability of HeLa and human keratinocyte (HaCaT) cells in a dose-dependent manner. The dppz complex **3** showed enhancement in the cytotoxicity when irradiated with UV-A or visible light. The dark toxicity of the complex seems to be significantly lower than that shown in the presence of UV-A or visible light. The dppz complex shows more than a 20-fold increase in the cytotoxicity in the HeLa cells upon irradiation with visible light (400−700 nm) and more than a 200-fold increase in UV-A light (365 nm) compared to the nonirradiated samples. Similar results were obtained with the HaCaT cells with a more than 20-fold increase in cytotoxicity with visible light and a more than 100-fold increase on UV-A irradiation. No reduction in cell viability was observed upon treatment of the cells with only the light sources (UV-A and visible light). The IC_{50} values of **3**, Photofrin, and cisplatin in the HeLa and HaCaT cell lines are tabulated in Table 4. Cisplatin, the most successful and most frequently prescribed metal-based anticancer drug, suffers from severe dose-limiting side effects that result in treatment failure. Moreover, tumors possess intrinsic or acquired resistance to these drugs. An iron-based prodrug

(73) Thompson, K. H.; Orvig, C. *Dalton Trans.* **2006**, 761–764.
(74) Peters, T. *Adv. Protein Chem.* **1985**, *37*, 161–245.
(75) Halfman, C. T.; Nishida, T. *Biochim. Biophys. Acta* **1971**, *243*, 284–293.
(76) Halfman, C. T.; Nishida, T. *Biochim. Biophys. Acta* **1971**, *243*, 294–303.
(77) Sarkar, B. *Biol. Trace Elem. Res.* **1989**, *21*, 137–144.

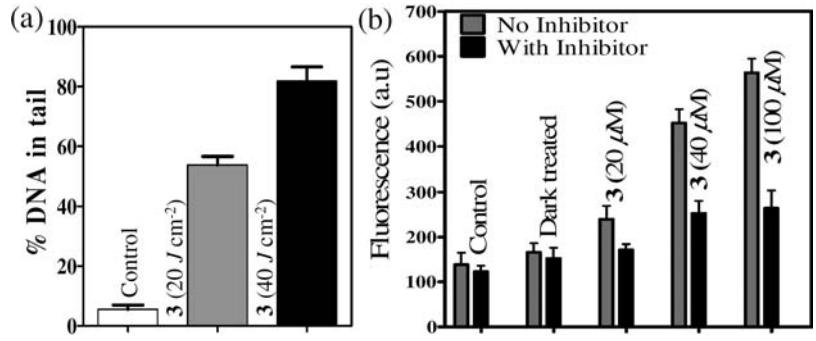

Figure 9. (a) Distribution of DNA damage in HeLa cells 2 h after photoexposure with complex **3** using visible light. Each histogram represents the mean ± s.d. ($n = 10$) of the %DNA in the tail in the control and treated cells. (b) PDT using visible irradiation with various concentrations of **3** in HeLa induces an increase in caspase 3/7 activity 2 h after photoirradiation, which is inhibited by general caspase inhibitor ZVAD-FMK (10 μM) added 30 min before photoirradiation. The DEVD-ase cleavage activity has been measured using a cell-free protease assay (each histogram represents the mean ± s.d. ($n = 3$)).

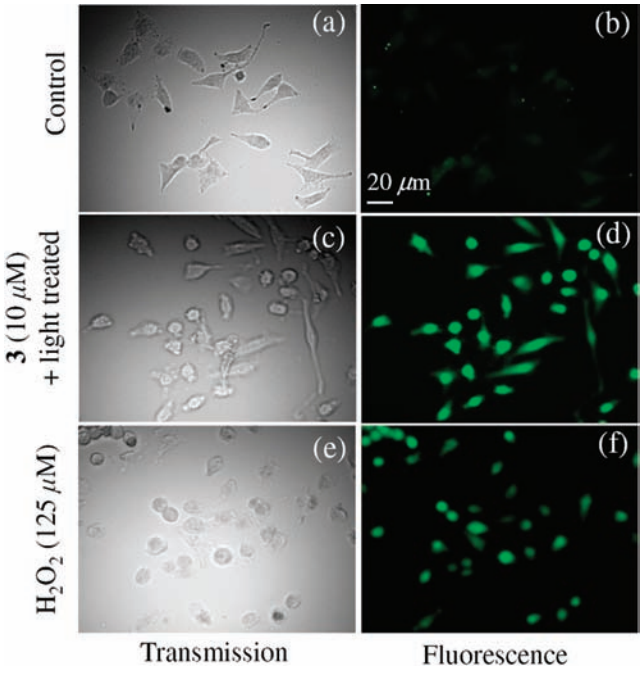

Figure 10. HeLa cells showing an increase in the ROS levels upon treatment with complex **3** (10 μM) and visible light (400−700 nm, 20 *J* cm^{-2}) (panels c and d) as compared to the untreated photoirradiated control cells (panels a and b). Cells have been treated with 125 μM H_2O_2 for 30 min as a positive control (panels e and f). Panels b, d, and f were acquired using fluorescence microscopy with 485/20 nm excitation and 535/40 nm emission filter sets after incubating the cells with 25 μM DCFH-DA for 30 min following appropriate treatment, while panels a, c, and e show the bright field images (transmission).

that is relatively nontoxic in the dark, but is only activated by light to produce cytotoxic hydroxyl radicals, could serve as a potent metal-based PDT agent. It could overcome the acquisition of resistance that arises in the case of cisplatin and other platinum-based drugs. Moreover, the inherent toxicity of the heavy metals could also be circumvented with the relatively nontoxic iron-based drugs.

Photodynamic Effect on Nuclear Morphology. Hoechst staining and AO/EB dual staining have been done to ascertain whether the cell death induced by complex **3** involves changes in nuclear characteristics. To identify the possible involvement of apoptosis, the visible-light-irradiated HeLa cells treated with complex **3** (10 μM for 4 h in dark) were stained with Hoechst 33258 or AO/EB dual stain. A significant increase in the apoptotic nuclear morphology such as extensive chromatin aggregation or nuclear condensation was observed in the treated cells (Figure 8c) as compared to the evenly stained nuclear contours of the normal HeLa cells (Figure 8a) or nonirradiated controls (Figure 8b) upon Hoechst 33258 staining. The control cells that stained evenly with Hoechst were also found to stain lightly and evenly with AO but stained negative for EB, suggesting the presence of live cells (Figure 8d). This can be explained by the fact that, though both of these dyes intercalate DNA, only AO can cross the plasma membrane and stain the cells, whereas ethidium bromide is actively excluded from the cells having an intact plasma membrane.[78,79] On the other hand, treated HeLa cells after 1 h of postirradiation displayed intensely stained green nuclei, a characteristic of the early apoptotic cells (Figure 8e). This intense staining is the result of chromatin condensation without a loss in membrane integrity (hence, EB-negative). After 2 h of postirradiation, the cells exhibit a condensed orange nucleus (Figure 8f), a hallmark of late apoptotic cells, whereas the necrotic cells display a structurally intact nucleus with even orange staining. The orange nucleus is due to the loss of membrane integrity in the late apoptotic and necrotic cells that allows EB to stain the nucleus.

Fragmentation of Nuclear DNA by Comet Assay. The alkaline single cell gel electrophoresis (SCGE) or Comet assay gives an image of the changes that have occurred in the chromatin organization in a single cell following PDT, which is considered a more accurate way of detection of early nuclear changes in a cell population.[80] When complex **3** was photoactivated in the HeLa cells by visible radiation (20 *J* cm^{-2}) and analyzed by alkaline single-cell gel electrophoresis, more than 50% of the DNA was found in the tail, consisting of low-molecular-weight DNA (Figure 9a, Figure S19 in Supporting Information). With higher doses of radiation (40 *J* cm^{-2}), nearly 85% of the genomic DNA migrated to the tail, whereas the nontreated controls showed

(78) Renvoize, C.; Biola, A.; Pallardy, M.; Breard, J. *Cell Biol. Toxicol.* **1998**, *14*, 111–120.
(79) Ribble, D.; Goldstein, N. B.; Norris, D. A.; Shellman, Y. G. *BMC Biotechnol.* **2005**, *5*, 12–18.
(80) Rousset, N.; Keminon, E.; Eleouet, S.; Le Neel, T.; Auget, J. L.; Vonarx, V.; Carre, J.; Lajat, Y.; Patrice, T. *J Photochem. Photobiol. B* **2000**, *56*, 118–131.

only 5% DNA in the tail and 95% migrating as the intact head, corresponding to normal high-molecular-weight DNA. The outcome of the Comet assay shows that a single cell's DNA underwent degradation as a consequence of direct DNA damage or rapid apoptosis (evident from the nuclear staining) induced upon photoexposure following treatment with complex **3**.

ROS Generation. The photoirradiated HeLa cells showed significantly higher levels of ROS, as indicated by DCF generation in the cells. As shown in Figure 10b, the untreated control cells appear unstained or very lightly stained, while the cells treated with both complex **3** and visible light (Figure 10d) showed an increase in levels of DCF fluorescence. As a positive control, the HeLa cells were exposed to 125 μM H_2O_2 for 30 min, which showed significant DCF staining as well (Figure 10f). Phase contrast microscopy revealed that the morphological features of complex **3**-treated cells (Figure 10c) appeared similar to the H_2O_2-treated cells (Figure 10e) characterized by membrane blebbing and cell shrinkage, while the untreated controls (Figure 10a) did not resemble complex **3**-treated cells. Quantification of the above results using fluorimetry showed 2-, 4-, and 8-fold increases in DCF fluorescence for the cells treated with 5, 10, and 20 μM complex **3**, respectively, as compared to the light-treated controls. These data resemble the results obtained with inhibitor studies in DNA photocleavage (Figure S20 in the Supporting Information). The results are in good agreement with the EPR spectral data showing DMPO−HO$^{\bullet}$ formation (Figure S16a in Supporting Information). Thus, the oxidative stress due to ROS generation by complex **3** on photoexcitation may contribute largely to the cell death.

Caspase 3/7 Involvement in Cell Cytotoxicity. Evidence from the nuclear staining and phase contrast picture of the HeLa cells following photoexposure overwhelmingly suggested that complex **3** induced apoptosis, characterized by nuclear condensation, cell shrinkage, and surface blebbing. This was further confirmed by determining the activities of caspase 3/7, 2 h after treatment that increased in a dose-dependent manner following photoirradiation. The untreated controls and the dark controls showed no caspase 3/7 activity. The specificity of cleavage activity was confirmed by pretreating the cells with a 10 μM general caspase inhibitor ZVAD-FMK prior to irradiation, which resulted in partial neutralization of caspase 3/7 (Figure 9b). Apoptosis, unlike necrosis, does not induce any host immune response and toxic effects to the surrounding normal tissues and hence is more tolerable to patients.[81,82] It must be noted that the presence of a general caspase inhibitor was unable to completely block caspase 3/7 activity, suggesting the fact that the caspase 3/7 pathway might not be the sole pathway for the observed cytotoxicity.

Conclusion

We report here a new class of ternary iron(III) complexes having a tetradentate phenolate-based ligand and phenanthroline bases designed for cellular studies in PDT. The complexes show efficient DNA and protein (BSA) binding propensities. The complexes show photoinduced DNA cleavage activity in visible light via a mechanistic pathway that involves the formation of hydroxyl radicals. This is in contrast to the organic porphyrin and phthalocyanin dyes that are known to photocleave DNA via a singlet oxygen pathway. The ternary iron(III) complexes in the dark or their constituents alone in the light are cleavage-inactive. The complexes do not show any BSA cleavage on exposure to light, and thus the protein could act as a carrier of the complex molecules. The complexes are potent pseudo-photonucleases rather than photochemical proteases. The visible-light-induced DNA cleavage involves a phenolate-to-iron(III) LMCT band in the metal-assisted photosensitization process, giving the extent of cleavage as dppz complex $\geq$ dpq complex $>$ phen complex. The percent SC DNA cleavage observed at different wavelengths follows the visible spectral band pattern.

Evaluation of the photocytotoxic property of complex **3** on HeLa and HaCaT cells revealed that complex **3**, which is nontoxic in the dark, becomes potentially cytotoxic upon irradiation with visible or UV-A light. The IC_{50} values of complex **3** are marginally higher in HaCaT than in HeLa cells. Complex **3**, possessing low dark toxicity, is a useful candidate for future iron-based photodrug development. Rapid changes in nuclear morphology are noticed with Hoechst staining, which was confirmed by acridine orange/ethidium bromide staining, revealing the fact that most of the cells enter early apoptosis within 2 h of light treatment. Caspase 3/7 activity is also upregulated, indicating programmed cell death to be the predominant form of cell death induced by complex **3** and visible light. Extensive ROS generation has also been detected by dichlorofluorescein staining that possibly induces apoptosis by direct DNA damage, as evidenced from the alkaline comet assay. In summary, we present an iron-based complex that shows low dark toxicity but significantly high photocytotoxicity, thus making this complex a potent PDT agent for anticancer applications, especially for skin cancer.

Acknowledgment. We thank the Department of Science and Technology (DST), Government of India, and the Council of Scientific and Industrial Research (CSIR), New Delhi, for financial support (SR/S5/MBD-02/2007 and 01(2081)/06/EMR-II) and DST for the CCD diffractometer facility. The authors thank Prof. Annapoorni Rangarajan (MRDG, IISc) for the fluorescence microscopic facility. HaCaT cells were a gift from Prof. Paturu Kondaiah (MRDG, IISc), and the authors sincerely thank him for helpful discussions. We thank Dr. Ashis K. Patra and Dr. Munirathinam Nethaji for their help in structural studies. We are grateful to the Alexander von Humboldt Foundation, Germany, for an electrochemical system and the Convener, Bioinformatics Center of our Institute, for database search.

(81) Zitvogel, L.; Casares, N.; Pequignot, M. O.; Chaput, N.; Albert, M. L.; Kroemer, G. *Adv. Immunol.* **2004**, *84*, 131–179.
(82) Melcher, A.; Gough, M.; Todryk, S.; Vile, R. *J. Mol. Med.* **1999**, *77*, 824–833.

S.S. thanks CSIR for the fellowship. A.R.C. thanks DST for a J. C. Bose National Fellowship. We thank the reviewers for their valuable comments.

Supporting Information Available: Detailed description of X-ray crystallographic procedures and experimental methods used for DNA binding, DNA photocleavage, and cell cytoxicity studies (5 pages); ESI-MS (Figures S1−S3) and UV−visible spectra (Figures S4, S5); cyclic voltammograms (Figure S6); ORTEP and unit cell packing diagrams (Figures S7−S10); DNA binding and cleavage (Figures S11−S16); protein binding and cleavage (Figure S17); MTT assay for complex **2** (Figure S18); SCGE and ROS quantification (Figures S19, S20); and mechanistic scheme (Scheme S1). Crystallographic data in CIF format for complexes **1** and **3** along with selected bond distances and angles (Tables S1, S2). This material is available free of charge via the Internet at http://pubs.acs.org.

IC8022612